Fire Safety Journal 162 (2026) 104666

Contents lists available at ScienceDirect

Fire Safety Journal

journal homepage: www.elsevier.com/locate/firesaf

Characterizing the hazards of vehicle fires in the WUI[☆]

Giovanni Di Cristina [*], Aika Davis, Matthew Bundy, Anthony Hamins

Fire Research Division, National Institute of Standards and Technology, 100 Bureau Dr., Gaithersburg, MD, USA

A R T I C L E I N F O

Keywords:
WUI fires
Fire emissions
Heat release rate
Vehicle fires
Calorimetry

A B S T R A C T

The burning characteristics and hazards associated with three types of vehicles in the context of a wildland–urban interface (WUI) fire were examined. The experiments were conducted under the 20 MW calorimeter hood at the National Institute of Standards and Technology (NIST). The calorimeter provided well-characterized heat release rate measurements. Additional gas sampling measured the yields of thirteen species in the combustion gasses. Measurements of the near- and far-field heat flux to the surroundings are used to examine the risks posed to hypothetical surrounding structures or vehicles. Finally, soot was collected on a filter and was analyzed for polycyclic aromatic hydrocarbons and select elements using gas chromatography mass spectrometry and combustion ion chromatography, respectively. The data generated from the study will be included in the NIST Fire Calorimetry Database (FCD). The measurements characterize the global combustion properties of the vehicles and offer insight into their burning behavior, risk posed to surrounding structures and fuels, and their effluent smoke constituents.

1. Introduction

As wildland–urban interface (WUI) areas increase [1], there is a growing need for further quantification and mitigation of fire hazards in the WUI. In 2024, over 4500 structures were destroyed due to wildland fires in the United States, including over 2400 residential structures [2]. In 2023 suppression alone cost the U.S. federal government $3.16 billion [3], well above the 5- and 10-year averages.

Structures in WUI can ignite via multiple pathways [4–6]. Commonly, firebrands (embers) are lofted in the air and land on combustible fuels near a structure, such as a shed or landscaping vegetation, creating secondary fires which eventually cause the structure to ignite. Vehicles, which are typically parked close to structures, another vehicle, or other fuel sources, pose a hazard to WUI structures as they can be a mechanism by which the smaller secondary fires lead to structure ignition and fire spread within a community [5]. There is an entire technical literature devoted to experiments and modeling of wildland fire fuels, particularly pine needles [7,8]. Pine needles are a fine fuel that can easily ignite and burn fast. In regions such as the western United States, the accumulation of pine needles in proximity to structures and vehicles represents a significant ignition vulnerability. These fuel beds are particularly hazardous because they can be ignited by firebrands or embers transported by convective columns from wildfires as distant as 40 miles [5,6,9].

Although studies have been conducted examining the heat release rate (HRR) and energy content of vehicles [10–16], these studies are targeted for the urban environment, in particular, parking garages or tunnels.

The ignition methods vary broadly, ranging from a pilot flame placed inside the vehicle (passenger or engine compartment), small fires set against the chassis, and fires underneath the fuel tank [10,13–17]. The ignition method consequently has a significant impact on the HRR and fire behavior. Typically vehicle fires initiated underneath the vehicle have the largest peak HRR while those initiated inside the vehicle have less variability in the peak HRR. Total heat released can vary as well, although the values are similar across ignition methods. Finally, the fastest time to peak HRR typically is seen with vehicle fires initiated along the chassis [17]. While previous burn experiments of vehicles often used mass loss as a surrogate for HRR [14,15], this study aims to conduct experiments which simulate vehicle fires in a WUI scenario under a well characterized oxygen consumption calorimeter [18].

Understanding the threat posed by vehicles is of interest for fire protection analysis and research, including fire model reconstruction of WUI events and hazard mitigation strategies [5]. In this study, three vehicle experiments were conducted underneath the National Institute of Standards and Technology's (NIST) 20 MW calorimeter hood, which provides HRR measurements with well characterized uncertainty. Each vehicle was ignited via a pine straw line fire to simulate a WUI ignition scenario, in the context of other vehicle fires, the ignition scenario will initiate with flames impinging on the chassis and transition into

☆ This article is part of a Special issue entitled: 'FISJ_IAFSS 2026' published in Fire Safety Journal.

* Corresponding author.
E-mail address: giovanni.dicristinatorres@nist.gov (G. Di Cristina).

https://doi.org/10.1016/j.firesaf.2026.104666
Received 24 September 2025; Received in revised form 13 February 2026; Accepted 22 February 2026
Available online 24 February 2026
0379-7112/Published by Elsevier Ltd.

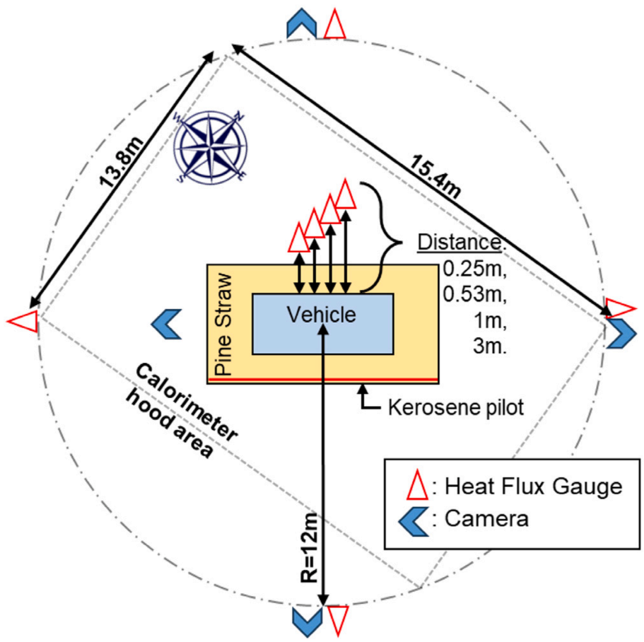

Fig. 1. Schematic of the vehicle fire experimental setup showing the instrumentation locations along with the hood area and camera locations.

flames underneath the vehicles as the pine straw surface fire spreads along the fuel bed. Measurements of heat flux inform the impact to structures or other vehicles. The temperature throughout each vehicle was measured to determine how the fire spread once the vehicles were ignited. Finally, gas and particulate sampling from the effluent quantify the toxicity of vehicle fire effluent to the surroundings.

2. Experimental setup and methods

An experimental setup was designed in order to characterize the risk of vehicle fires in a WUI scenario. Three different vehicle types were tested. The vehicles were placed on a pine needle bed situated beneath the 20 MW calorimeter hood of the National Fire Research Laboratory (NFRL) at NIST [18]. The pine needles were approximately 10 cm in length with an average moisture content of 11.8% and served as the ignition source of the vehicle. The pine straw bed area extended approximately 0.6 m in each direction beyond the vehicle perimeter. A pine straw fuel loading of 1.2 kg/m^2 was utilized with a total fuel mass of 21 kg. Pilot ignition of the pine straw was achieved with 1 L of Kerosene (0.8 kg) poured along a wick the length of the pine straw bed. A pine straw line fire was formed from the piloted ignitions simulating an approaching surface fire, which subsequently spread and ignited the vehicles.

Each vehicle was instrumented with eighteen thermocouples (bare bead, Type K) to measure the temperature and fire spread throughout the engine, passenger, and rear (trunk or rear passenger) compartments. Heat flux sensors were placed at near- and far-field locations. Near-field measurements were taken at 0.25 m, 0.53 m, 1 m, and 3 m standoff distances from the side of the vehicle, at a height of 1.5 m. At the 0.25 m and 0.53 m sensor locations, water cooled Schmidt–Boelter type heat flux gauges were utilized, while at the 1 m and 3 m locations, plate thermometers (PTs) were used with which the incident heat flux was calculated using the 1-dimensional heat transfer model methodology in Wickstrom [19,20]. The near-field measurements represent the risks to nearby structures or other vehicles. Far-field heat flux was measured at a radial distance of 12 m from the center for the vehicles and placed with views covering each side of the vehicles also at a 1.5 m height. The far-field measurements are useful for characterizing the radiant fraction, as well as generating data sets for fire model validation. Four cameras were utilized to record the experiments from the front, sides, and below the vehicle. A schematic of the experimental setup is shown in Fig. 1. Instrumentation was connected to a data acquisition system (DAQ) sampling at 1 Hz.

Specifications of the three vehicles used are summarized in Table 1, including dimensions (length × width), initial mass, and vehicle type. All vehicles had internal combustion engines (ICE); however, vehicle 3 (V3) was an electric hybrid model, which had the hybrid motor battery removed prior to the experiment. In all vehicles, the shocks, struts, and tires were punctured to reduce the risk of overpressurization due to safety concerns. The vehicle body was lifted and placed on four small metal blocks (10 cm by 15 cm) to position the vehicle at its normal ground clearance to compensate for the deflated tires. The first vehicle (V1) was tested with an empty fuel tank, while the other two had fuel tanks half-filled with 87 octane (Anti-Knock Index) unleaded gasoline. The experiments were conducted with the vehicle windows closed. The engine antifreeze was present during the tests, but the air conditioning fluid was removed for V1 and V2 due to initial safety concerns. V3 had 0.43 kg of air conditioning fluid, refrigerant HFC R134a, present during the fire experiment. All other engine fluids (motor oil, transmission fluid, brake fluid, etc.) were left in the vehicles.

The experiments took place underneath the NFRL's 20 MW calorimeter hood [18]. The hood has an area of 15.4 m by 13.8 m, as shown in Fig. 1. The long axes of the vehicles were aligned with the diagonal of the rectangular exhaust hood area. The exhaust hood measurement system provides real time heat release rate (HRR) via oxygen consumption calorimetry. The calorimetry system utilizes gas analyzers to obtain volume fractions of oxygen (O_2), carbon dioxide (CO_2), and carbon monoxide (CO), by continuously sampling from the exhaust duct at a well-mixed downstream position [18]. At the same location, the calorimetry system uses thermocouples and annubars connected to capacitance manometers to determine the duct mass flow. A laser transmission measurement across the duct provides the concentration of soot [21]. A Fourier Transform Infrared Spectrometer (FTIR) was added to the calorimetry system's sampling line to measure trace gaseous species from the duct [22]. The FTIR data was averaged over 24 s to account for the gas residence time within the FTIR chamber.

2.1. Particulate matter sampling and analysis

Particulate phase smoke was sampled for V2 and V3 from a well-mixed position in the calorimeter's exhaust duct, similar to Davis et al. [23]. A sampling pump pulled smoke through a 47.0 mm quartz filter at 5 SLPM along with another bypass pump to meet isokinetic sampling conditions. The quartz filters were weighed before and after sampling, after conditioning in a desiccant for over 24 h to obtain the particulate matter (PM) mass collected on the filter.

PM collected on the quartz filters was analyzed for targeted polycyclic aromatic hydrocarbons (PAHs) and selected inorganic elements. For the PAH analysis, a fourth of the quartz filter was extracted with an accelerated solvent extractor (ASE, Thermo Scientific Dionex ASE 350[1]) using dichloromethane (DCM) [24]. The cut filters were heated to 150 °C, rinsed, then purged, repeating the cycle six times. The extracts were then spiked with NIST SRM 2269 and SRM 2270 and concentrated using a TurboVap LV evaporator (Zymark). Background filters were also extracted similarly.

The concentrated extracts were injected (2 μL) directly onto gas chromatography-mass spectrometry (GC–MS), analyzing for 29 PAHs

[1] Certain equipment, instruments, software, or materials, commercial or non-commercial, are identified in this paper in order to specify the experimental procedure adequately. Such identification does not imply recommendation or endorsement of any product or service by NIST, nor does it imply that the materials or equipment identified are necessarily the best available for the purpose.

Table 1
Summary of vehicle specifications, dimensions, pre-test mass, and other details. The combined expanded ($k = 2$) uncertainties are also listed.

Vehicle	Year	Type	Dimensions [m]	Initial mass [kg]	Fuel [L]	Notes
V1	2014	Sedan	4.50 × 1.75	1346 ± 20	none	
V2	2004	Minivan	4.40 × 1.73	1854 ± 4	45.4 ± 0.5	
V3	2010	Sedan (hybrid)	5.11 × 1.94	1328 ± 4	15.1 ± 0.5	Hybrid battery removed

ranging from anthracene to coronene. The GC–MS analytical and analysis methods are described in Davis et al. [25]. For total PAH mass fraction and yields, the individual PAH molar fractions and yields are normalized to the molecular weight of anthracene to be anthracene equivalent. All data reported are background corrected.

Semi-quantitative elemental analysis of bromine (Br), chlorine (Cl), fluorine (F), and phosphate (P) were determined with a combustion ion chromatograph (CIC, Metrohm Combustion Module P/N 2.136.0700 with ion chromatography 920 absorber Module 2.920.0010). One circular filter punch-out (4 mm diameter) was placed in a quartz boat and into an oven at 1050 °C. The combusted ions were retained in approximately 5 mL of an absorber solution containing 500 ppm H_2O_2 in deionized water. The absorber solution was then analyzed for Br, Cl, F, and P as PO43- using ion chromatography. More details of the CIC can be found in Davis et al. [24].

2.2. Ignition method

Preliminary experiments were conducted to characterize the WUI ignition scenario. The control experiments consisted of a 1.2 m by 2.4 m non-combustible gypsum board set 20 cm over the pine straw bed, to simulate the presence of a vehicle. Water cooled heat flux gauges were positioned flush with the bottom of the board in the center and near its edge. Three repeat experiments were conducted, and the values summarized below represent the average from the three preliminary experiments. The average duration of these fires was 13.8 min with a peak HRR of 1.45 MW ± 0.14 MW and a peak heat flux of 55.5 kW/m^2 ± 1.7 kW/m^2 incident on the bottom of the gypsum board, which mimicked the underside of a vehicle. These results provided confidence that a sufficient heat flux would be supplied to the underside of the vehicle to lead to ignition of thermoplastic vehicle components.

3. Results

From the time of ignition, it took about 1 min on average for the flames to impinge on the side of the vehicles. Once the flames impinged on the vehicle, exterior plastic components such as the bumper and door trim began to melt. Eventually, the flames reached the end of the pine straw bed between 4.5 min and 5.7 min after ignition. At this time, flames were spouting from the engine compartment and exterior components, which were heavily involved in the fire.

Loud bangs were heard and projectiles observed throughout the fires due to pressure release of airbags or possibly other pressurized vehicle systems. The fires were out between 94 min and 113 min after ignition, with a small amount of what appeared to be magnesium continuing to burn near the steering column in front of the driver's seat in all three experiments. Just after the end times shown in Fig. 2, the glowing magnesium was removed from the vehicles, and water was applied to the vehicle carcass to extinguish any remaining embers.

It is important to note that at approximately 8 min in the V1 experiment and 13 min in the V2 experiment, the vehicles shifted due to a rapid pressure release, which subsequently caused a heat flux gauge stand to fall over. A timeline of the vehicle fires is shown in Fig. 2 for each of the three vehicle experiments.

3.1. Calorimetry

The transient HRR results from the calorimetry measurements for the three vehicles are plotted in Fig. 3. The vehicles had HRR peaks ranging from approximately 5 MW to 11 MW, with V2 reaching the highest peak. V2 also had the largest amount of total heat released (THR), determined as the integral of the transient HRR from ignition to fire extinguishment. V2 was the vehicle with the most mass and amount of gasoline in the fuel tank (45 L).

V2 exhibited typical, triangular shaped [26], HRR dynamics, characterized by a fast increase (growth phase) in HRR to a well-defined peak (fully-developed), followed by a long decay period where the HRR gradually fell. In contrast, V1 had a shorter-spanned rise in HRR to an initial local peak (at approximately 6 min), after which the HRR plateaued to a pseudo-steady fully-developed state, followed by a second peak at 18 min. The second peak was the absolute maximum HRR of V1. V2 seemingly fell somewhere between the behaviors of V1 and V3, with a somewhat defined peak exhibiting a brief steady HRR of approximately 8 MW. The variability in HRR behavior is a challenge for performance based design and fire protection, as design fire HRR curves are typically approximated with a growth phase proportional to t^2 or t^3 [27,28] up to a defined peak HRR, after which the HRR is modeled with a decaying exponential ($\exp(-t)$). In the context of this study, this approach works well for V2, but is of marginal accuracy when modeling V3 and, unable to capture the two maxima observed in V1.

The calorimetry results are summarized in Table 2, including the total mass loss and percent mass burned in the fires, and total heat released (THR). These results include the contributions from the pine straw. All the vehicles had a similar amount of mass loss (241 kg to 265 kg) and mass consumed (13 % to 19 %), as the bulk of the materials burned were the interior fabrics, plastics, and upholstery, which do not contain much mass in comparison to the metal chassis and engine. Additional items contributing to the fire would be the plastics found in the exterior (front and rear bumpers, trim, etc.) and engine compartment (hoses, cable insulation, etc.). The mass consumed results from this study align well with other vehicle fire studies, which have found that the percent of mass consumed was around 15 % to 25 % regardless of the initial vehicle mass [29]. The Peak HRR and THR, however, are harder to compare with other experiments as the data varies largely with vehicle type, materials, and experimental setup [16,29,30]. Comparing the present results to results from vehicles of the same class and initial mass compiled by various studies [16,29,30] shows that there is large variability of results in the literature. From statistical analysis and review of older vehicle experiments [16], the results presented here show larger peak HRR, faster times to peak HRR, and larger THR. Comparisons to a more recent compilation of vehicle fire experiments [29], showed that the V1 and V3 peak HRR and THR aligned well with results from the literature, while V2 was higher. Furthermore, the trend that percent of mass burned is largely invariant across vehicles is consistent. The average effective heat of combustion (HOC) of the three vehicles in this study was 31.9 MJ/kg ± 15%, which was within the range of previous fire studies of ICE vehicles [29].

3.2. Temperature

The temperature results are presented as the spatial average of four zones of the vehicle; engine, passenger-front, passenger-back, and rear (trunk). The results from each zone is the average of the measurements

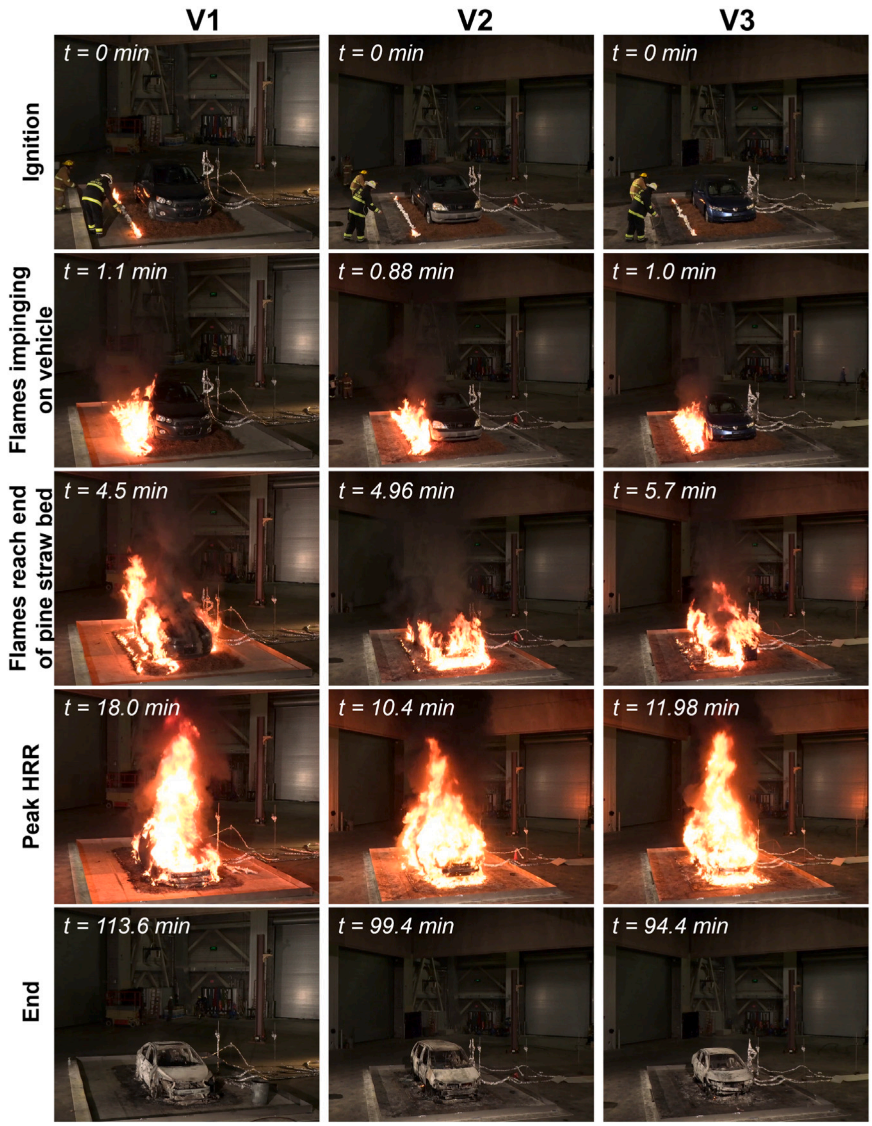

Fig. 2. Timeline images showing vehicle experiments V1 to V3 (left to right) key points: Ignition, initial flame impingement, flames reaching the end of the pine straw bed, peak HRR, and the end of each experiment.

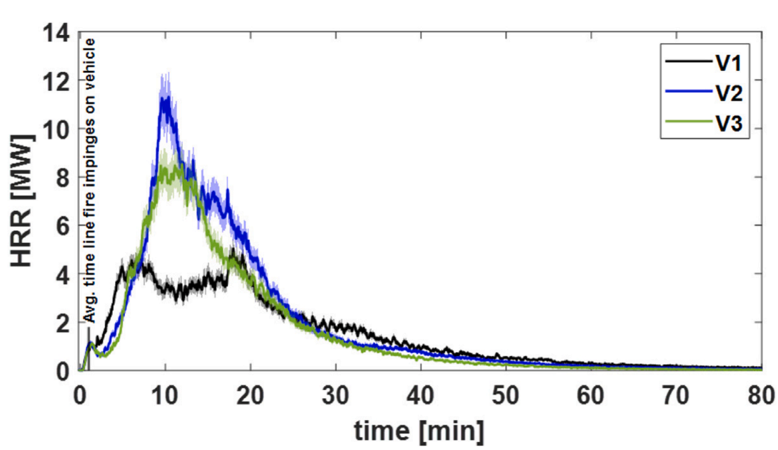

Fig. 3. Heat Release Rate for the three vehicle fires, the shaded region shows the expanded measurement uncertainty. $t = 0$ represents ignition of the pine straw.

from four thermocouples (TCs). In the engine compartment, each TC was positioned inboard of the edge by a fourth of the length and width of the bonnet dimensions. In the passenger compartments, TCs were placed centered at the roof and floorboard of each passenger station. In the rear, the TCs were centered depth-wise, in-line with the passenger stations, with TCs on the floorboard of the trunk and on the door. The

Table 2
Calorimetry results summary for the three vehicle fire experiments. Uncertainties represent a 95% confidence interval.

Vehicle	Mass Loss [kg]	% Mass Burned	Peak HRR [MW]	Time to Peak HRR [min]	Total Heat Released [MJ]	Effective HOC [MJ/kg]
V1	265 ± 28	19	5.0 ± 0.3	18.0 ± 0.2	7140 ± 450	26.9 ± 3.3
V2	257 ± 6	14	11.3 ± 0.7	10.4 ± 0.2	9330 ± 580	36.3 ± 2.4
V3	241 ± 6	18	8.5 ± 0.5	11.98 ± 0.2	7820 ± 490	32.4 ± 2.2

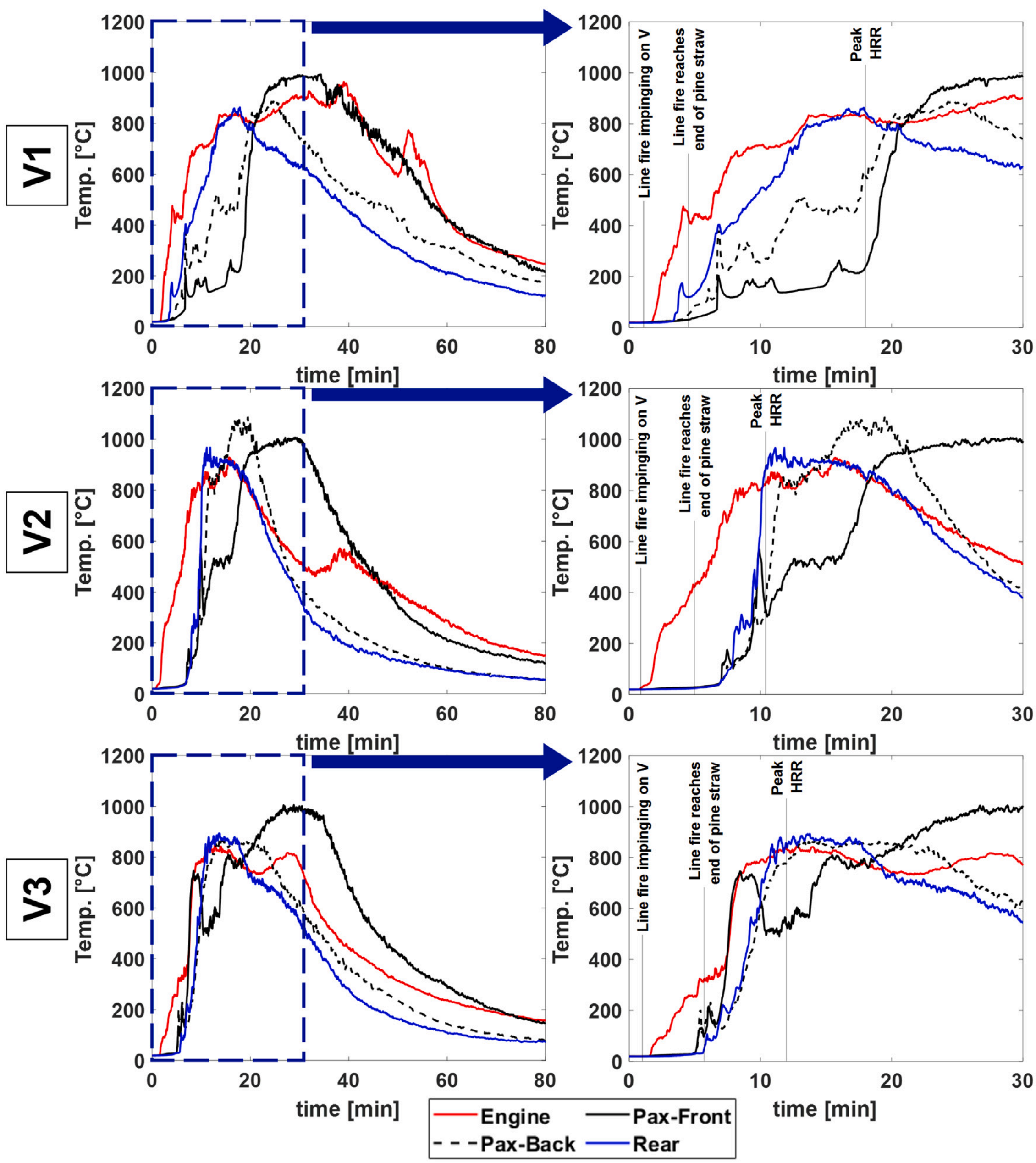

Fig. 4. Average temperatures from the engine, front passenger, back passenger, and rear compartments for each of the vehicles.

spatially averaged temperatures in the four zones are shown in Fig. 4 for all three vehicles, with the plots on the right showing a portion focused on the first 30 min.

The temperature in the engine compartment is the first to increase for all three vehicle fires, typically beginning to increase approximately 1 min after flames impinged on the vehicle. V1 and V3 showed a second sharp increase in engine temperatures around 6 min, while V2 exhibited a more steady temperature rise, likely due its larger volume of the engine compartment. The engine compartment temperatures reached a pseudo-steady state of approximately 800 °C before the peak HRR occurred.

The temperature in the passenger and rear compartments began rising around the time when the pine straw line fire reached the other end of the pine straw bed, at which point the engine was exhibiting temperatures between 300 °C and 400 °C. The rear compartment reached its peak sustained temperatures faster than the passenger compartments. Additionally, the rear peak sustained temperatures matched or slightly exceeded the highest engine temperatures.

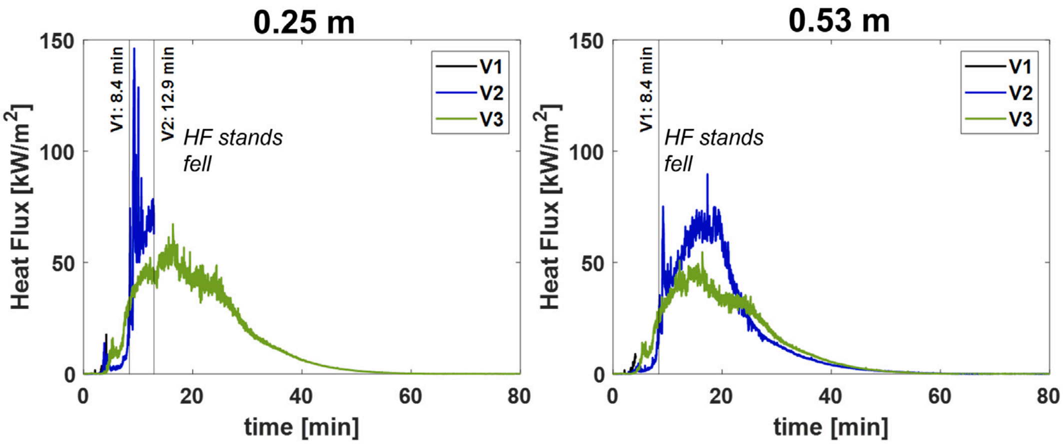

Fig. 5. Near-field heat flux measurements from the heat flux gauges.

Lastly, the temperature at the rear row of seats in the passenger compartment (Pax-Back in Fig. 4) rose earlier than the front row (Pax-Front). This is likely due to flames and heat penetrating the passenger compartment from the rear (trunk), as typically only seats or plastic trim separate the passenger and rear compartments, as opposed to the firewall, which separates the engine compartment from the rest of the vehicle. Although the passenger compartments as a whole were the slowest to heat up, they attained the highest observed temperatures of all the compartments, around 1000 °C. The peak passenger compartment temperatures were attained after peak HRR. Finally, low variation in the temperature was found between the left and right sides of the vehicle. This symmetry suggests that although the line fire spread from left to right with respect to the vehicles, the flame spread occurred from the front and rear of the vehicle inward.

3.3. Heat flux

3.3.1. Near-field

The near-field heat flux was measured at 0.25 m, 0.53 m, 1 m, and 3 m distances to provide estimates of the impinging heat flux on a potential nearby vehicle or structure. The 0.25 m and 0.53 m measurements from the heat flux gauges are shown in Fig. 5 and the 1 m and 3 m results measured with the PTs are in Fig. 6. Although PTs typically have a slower time response than the Schmidt–Boelter type gauges, this limitation is not an issue since the experiments were on the scale of hours and detailed transient dynamics are not examined at this time.

Unfortunately, in the V1 and V2 tests, some gauges fell over. Vertical lines have been added to the figures, identifying when the gauges fell over. During V1, both the 0.25 m and 0.53 m gauges fell over. Although they were still recording data, they were not pointing towards the fire. Only the 0.25 m gauge fell during the V2 test. The data traces from the fallen gauges have been truncated to only show data before their fall.

The heat flux trends in Figs. 5 and 6 align with the calorimetry trends shown in Fig. 3 and Table 2. That is, V2 had the highest peak heat flux values, followed by V3, with V1 assumed to be the lowest due to the 0.25 m and 0.53 m gauges falling mid-test. The peak heat flux values are summarized in Fig. 7, showing an approximately $1/r^2$ dependence with distance from the vehicles and with V2 consistently exhibiting the highest heat flux measurements across the different measurement locations. As a reference frame, the largest peak near-field HF observed during the preliminary pine straw fires was approximately 7 $\mathrm{kW/m^2}$ at 0.25 m.

Studies have derived a critical heat flux at which certain exterior vehicle components of a neighboring vehicle will ignite and subsequently spread across the entire vehicle [31]. This critical heat flux was determined to be between 10 $\mathrm{kW/m^2}$ and 20 $\mathrm{kW/m^2}$ depending on the assumptions made and the specific part of the vehicle which is exposed. For WUI structural components, critical heat fluxes of 20 $\mathrm{kW/m^2}$ would pose a risk to vinyl siding or fencing, plastic trash or recycling bins, and other plastic materials commonly found near and outside homes [4,5]. Finally, thick wood or other cellulosic materials could be at risk with heat fluxes above 45 $\mathrm{kW/m^2}$. For each of the three vehicles, the length of time that each heat flux measurement location was above 10 $\mathrm{kW/m^2}$, 20 $\mathrm{kW/m^2}$ and 45 $\mathrm{kW/m^2}$ was calculated and is shown in Fig. 8.

During the V2 fire, the near-field heat flux measurements surpassed critical values at nearly all the measurement locations, including at 0.53 m from the vehicle, where heat fluxes were above 20 $\mathrm{kW/m^2}$ for 17 min. Further, although V3 was a smaller vehicle with a less energetic fire, heat fluxes at 0.53 m were above 10 $\mathrm{kW/m^2}$ and 20 $\mathrm{kW/m^2}$ for longer than during the V2 fire. Times above 45 $\mathrm{kW/m^2}$ were fairly low in comparison, with significant time above the threshold observed mainly at the 0.25 m and 0.53 m distances. Radiation is a strong function of distance; accordingly, the times above critical heat flux diminish as the distance from the vehicle increases. Beyond 1 m, the times above critical heat flux values drop significantly. Within 1 m, the hazards to flammable structures, materials, or other vehicles in the WUI are high and are likely to ignite [6].

3.3.2. Far-field

The near field heat flux measurements provide insight as to what nearby objects or other vehicles may experience in terms of heat flux or likelihood of ignition. The measurements from the far-field heat flux gauges (at 12 m) help in determining the total radiated energy (TRE) to the surroundings. The transient far-field heat flux measurements are shown in Fig. 9 for each of the three vehicles. The average relative humidity of the lab during the experiments was 78 %.

For each of the tests, the measurements from each of the four far-field measurement locations should be nearly identical, as they were far enough away from the fire such that they should capture all the radiated energy. In practice, however, that is not the case. Particularly for the V1 data, the southeast (SE) location generally measured a higher heat flux than the other locations. The disparity is most likely due to the pilot ignition location, which occurs on the side facing the SE gauge. Although this trend remains in the V2 and V3 experiments, V1 is the most disparate. Generally, as expected, the far-field heat fluxes seen in Fig. 9 roughly follow the HRR trends seen in Fig. 3. This relationship is shown in Fig. 10, which plots the average of the peak far-field heat flux from each location (NE, SE, SW, NW) as a function of peak HRR. At the far-field, the preliminary pine straw fires were observed to have peak heat fluxes lower than 0.35 $\mathrm{kW/m^2}$.

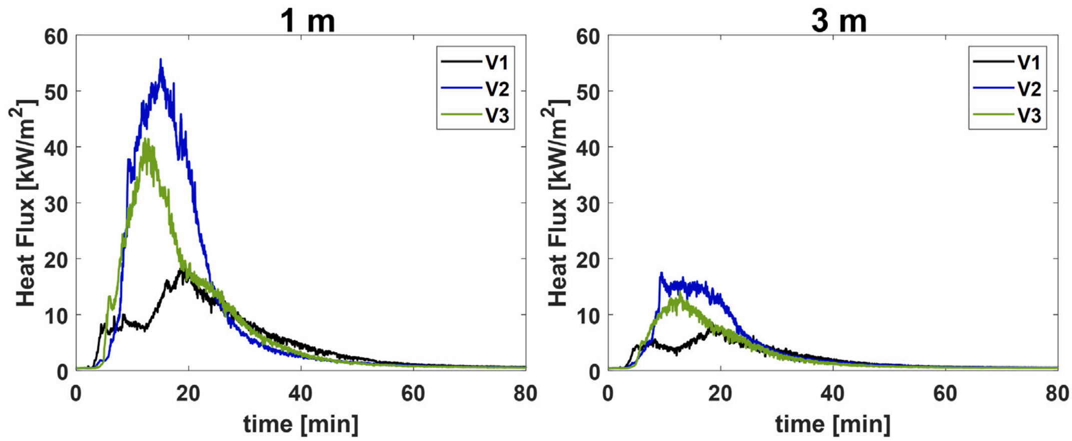

Fig. 6. Near-field heat flux calculated from the PT measurements.

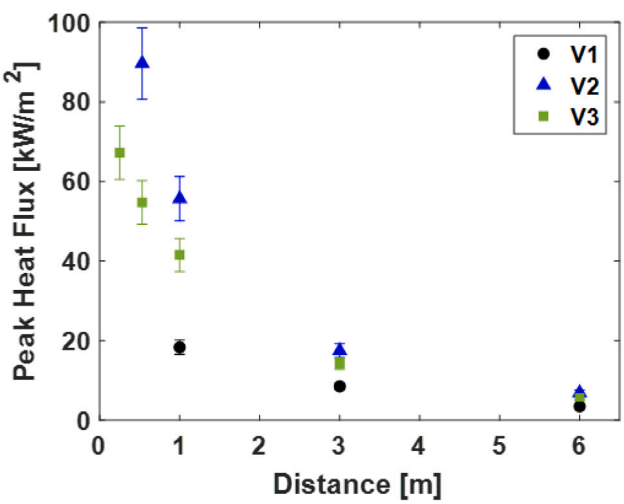

Fig. 7. Peak near-field heat flux as a function of distance measured for the three vehicles tested. Error bars represent the combined measurement uncertainty.

An estimate of the total radiative energy (TRE_i) was determined by integrating the measured radiative heat flux over the burning period (from ignition $t = 0$ to extinguishment $t = t_e$) at each of the measurement locations (NE, SE, SW, NW):

$$TRE_i = \int_0^{t_e} 4\pi \ R_i^2 \ \dot{q}_i'' \ dt \tag{1}$$

where ($\dot{q}_i''$) is the radiative heat flux measured at a distance (R_i) from the fire at the ith gauge. For suitably far distances from the fire, the ratio of the average total radiated energy to the surroundings and the measured energy released can be used to estimate the radiative fraction (χ_{rad}) of the fire as:

$$\chi_{rad} \approx \frac{\overline{TRE_i}}{\Delta m \ H_c} = \frac{\overline{TRE_i}}{THR} \tag{2}$$

where $\Delta \ m$ is the total mass loss, H_c is the net heat of combustion of the fuel, and THR is the total heat released (Table 2). The TRE from each measurement station along with the estimated χ_{rad} are summarized in Table 3. The average relative variance of the TRE measurements is approximately 31 %, however, if the SE measurements are excluded from the statistics, the relative average variance drops to 23 %. The radiative fractions are roughly the same for all three fires and are in line with other reported vehicle fires [32]. In general, these values are higher than canonical pool fires of similar size [33], which could be due to the re-radiation from the car surface itself, or the lab surroundings as the fires develop over a long period of time (see Table 3).

Table 3
Total Radiative Energy (TRE) determined from the four far-field measurement (r = 12 m) and χ_{rad} for each vehicle fire experiment.

	NE TRE [MJ]	SE TRE [MJ]	SW TRE [MJ]	NW TRE [MJ]	χ_{rad}
V1	2480	6950	4510	2710	0.58
V2	3990	5860	5040	3710	0.50
V3	3240	4990	4250	3170	0.50

4. Yields

4.1. Gas species yields

The yields of a range of gas species were determined from the FTIR tapped into the calorimetry's gas sampling line. First, the total mass generated of a given species, i, was calculated using Eq. (3):

$$m_i = \frac{W_i}{W_{air}} \sum_{t_{ign}}^{t_{out}} \left[X_i(t) - X_i^o \right] \dot{m}_e \Delta t \tag{3}$$

where the difference between the measured concentration, $X_i(t)$, and the initial concentration, X_i^o, is summed over the duration of the fire and multiplied by the mass flow rate, $\dot{m}_e$, in the duct. The quantity is then scaled by the ratio of the molecular weight of the species of interest, W_i, to that of air, W_{air}, since the mass flow of the exhaust can be assumed to be mainly air [18,22]. The species yield, Y_i, is then defined as the ratio of the total mass generated, m_i (determined from Eq. (3)), and the mass loss of the vehicle, m_{tot} (found in Table 2), such that:

$$Y_i = \frac{m_i}{m_{tot}} \tag{4}$$

A variety of species concentrations were measured, and their yields are presented in Fig. 11. These species were chosen for consideration due to their toxicity and/or prevalence in urban fires [34,35].

Overall, the yields for a given species differed from test to test. The average relative variance across all species from the three vehicle experiments was approximately 18 %. Although the FTIR was not utilized for the pine straw only experiments (Section 2.2), the average yields of CO_2, Soot, and CO were 1.4 kg/kg, 65 g/kg, and 10.6 kg/kg, respectively.

V2 produced the largest amount of soot (as measured by the light attenuation), carbon monoxide (CO), and hydrogen cyanide (HCN), consistent with the fact that the test had the largest peak HRR, possibly due to the additional gasoline in the fuel tank. Although V3 also

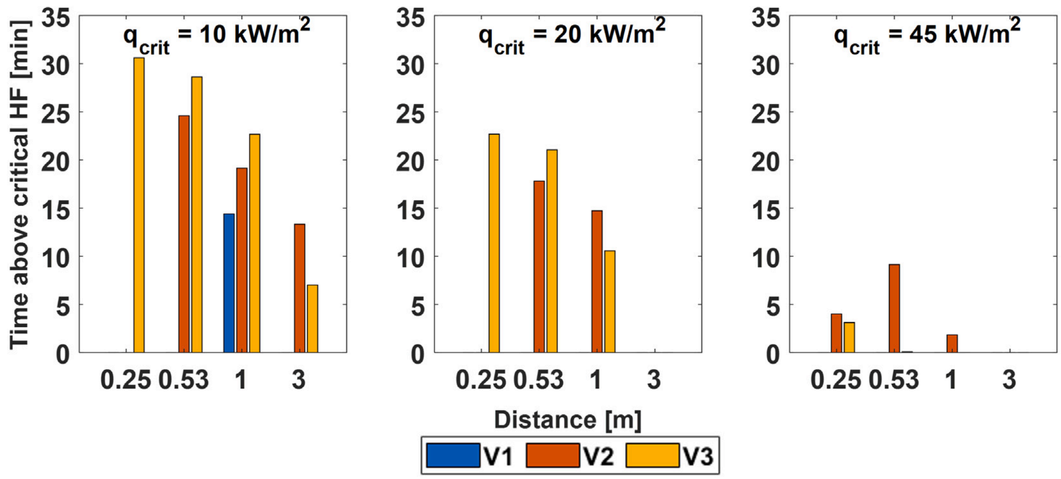

Fig. 8. Time (in minutes) where each heat flux measurement location is above the threshold values of 10 kW/m^2 (left), 20 kW/m^2 (center) and 45 kW/m^2 (right) for the three vehicle experiments.

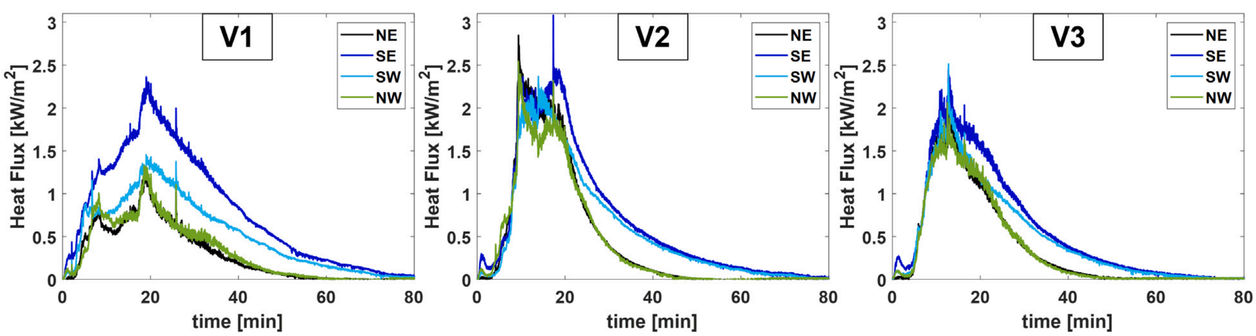

Fig. 9. Far-field heat flux for the three vehicles investigated.

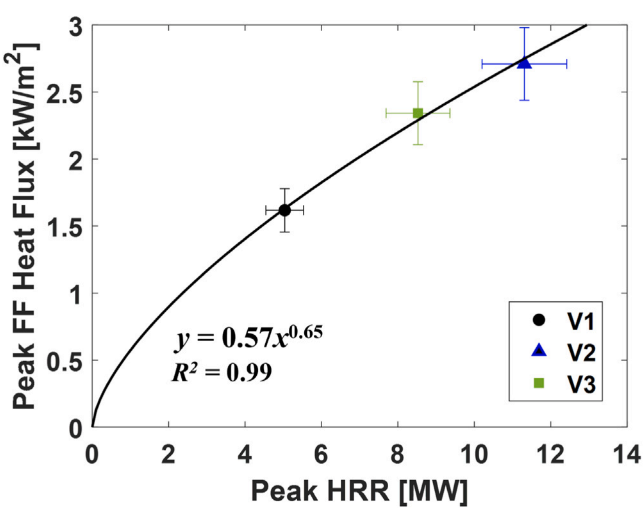

Fig. 10. Average peak far-field heat flux as a function of the peak HRR. The line shown is a power law fit with $R^2 = 0.99$.

had gasoline in the fuel tank, it was only 15 L compared to 45 L in V2. Lastly, other toxic hydrogenated compounds such as hydrogen bromide (HBr), hydrogen chloride (HCl), and hydrogen fluoride (HF) are expected to be present but were below the instrument detection limits, likely due to the dilution of the effluent by ambient air in the hood exhaust stream. However, halogenated elements were detected in soot (discussed in Section 4.2). The thirteen species observed and the total quantities emitted are slightly higher compared to what has been reported by other studies [30]. However, differences in experimental conditions and the composition of vehicle materials, including engine fluids, could strongly influence the total yields.

4.2. PAHs and inorganic elements in PM from smoke

Gravimetric PM yields based on PM mass collected on the filters for V2 and V3 are 0.066 kg/kg ± 0.005 kg/kg and 0.045 kg/kg ± 0.003 kg/kg, respectively. These results agree with the soot results from the smoke extinction measurement shown in Fig. 11. One reason for V2 having a higher PM yield may be due to its lower modified combustion efficiency (MCE), $Y_{CO}/(Y_{CO} + Y_{CO_2})$ [23,36]. V2 had an MCE of 0.978 ± 0.029 compared to 0.982 ± 0.033 for V3, thereby releasing more soot from incomplete combustion.

Since PAHs are the main precursors to soot formation [25], one may expect a higher total PAH yield for V2, which had a higher PM yield compared to V3. However, the total PAH yields in the smoke samples from the two vehicles are comparable (Fig. 12) with V3 being slightly higher.

The individual PAH yields, shown in Fig. 13, tend to be comparable between the two cars with a similar trend in PAH emission profiles; both have higher yields for lighter/lower molecular weight PAH compounds and lower yields for the heavier/longer PAHs. Individual PAH yields also show higher yields for V3 compared to V2 for all identified PAHs except for two (perylene and anthanthrene).

The mass fraction of PAHs in PM collected on the filters are presented in Fig. 14. Here, a higher total PAH mass fraction is observed for V3, indicating that more PAHs are released for the same amount of

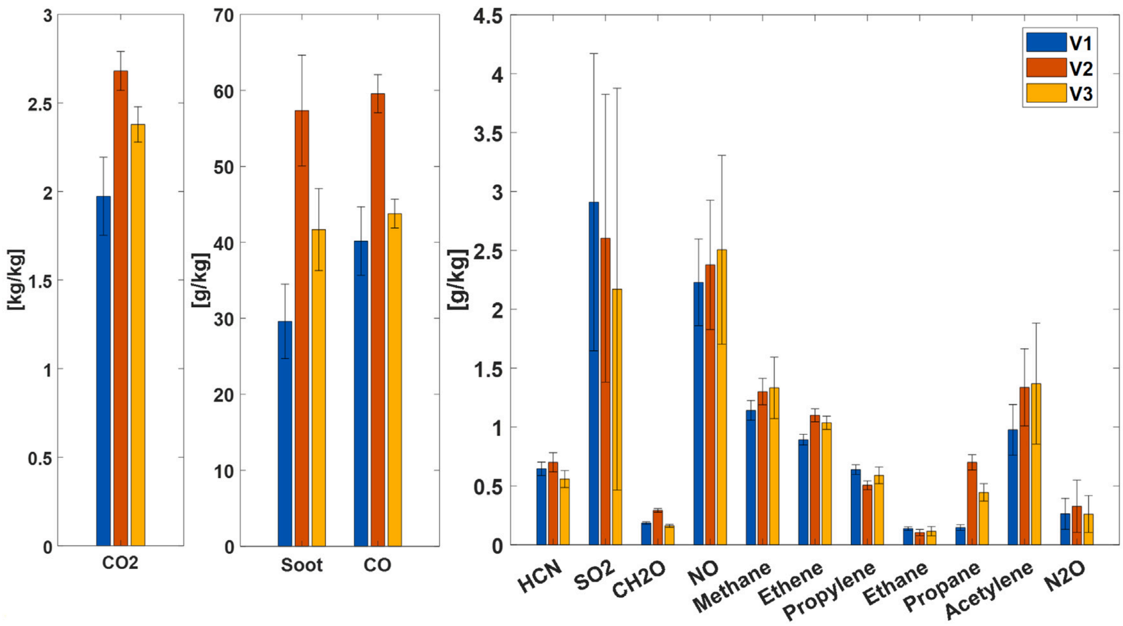

Fig. 11. Species yields and their uncertainty for a variety of compounds. Uncertainties are reported as the combined expanded ($k = 2$) uncertainty, representing a 95 % confidence interval.

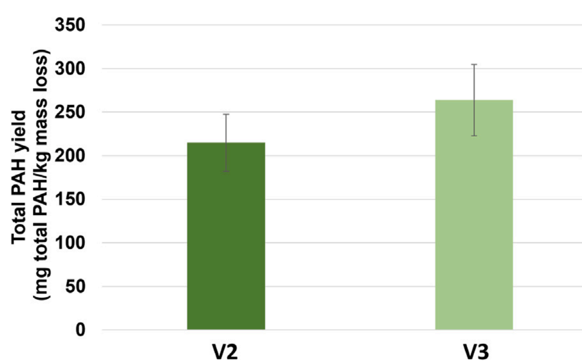

Fig. 12. Total PAH yields (anthracene equivalent) per kg of mass loss for V2 and V3.

PM released. This may be the reason why the PAH yields for V3 are higher despite it having a lower PM yield compared to those of V2.

Fig. 15 shows the yields of inorganic contents from V2 and V3. V2 and V3 had comparable yields of F, Br, Cl, and P. The highest detected halogen was Cl. Cl is likely coming from all the Polyvinyl Chloride (PVC) used in vehicle parts such as cable insulation, weatherstripping, instrument panel cover, HVAC parts, etc., which can contain PVC. F is found in vehicle parts that use fluoropolymers for heat and corrosion resistance such as engine tubing (fuel lines), o-rings, and gaskets. Finally, Br, Cl, and P could be from vehicle components, which require flammability-resistant features, such as the upholstery or other seat components.

5. Conclusion

The burning characteristics of vehicle fires were characterized, along with the hazards to surrounding structures, in the context of a WUI fire. Calorimetry data showed a wide range of characteristics, typical of the variability of vehicle fire data found in the literature due to the wide vehicle material composition, ignition methods, and lab conditions. However, some global trends were in agreement. Additionally, the calorimetry data expands the NIST Fire Calorimetry Database. Calorimetry data along with total radiated energy (TRE), are useful for performance-based designs and modelers looking to accurately capture vehicle fire dynamics. It was determined from the near-field heat flux measurements that structures or other fuel sources within 1 m of the burning vehicle are at a high risk of ignition. At this distance, heat fluxes above critical thresholds for ignition were sustained for 10 min to 22 min. Although at 3 m the sustained heat fluxes above critical thresholds were observed for shorter duration, they ranged from 7 min to 13 min in length and could still pose a risk. Lastly, the yields of 13 gaseous species of interest plus soot are reported based on FTIR measurements and particulate matter (PM) analysis determined that vehicles may release toxic and hazardous materials due to their complex material composition. The results of this study provide a robust data set for researchers and engineers, and inform future studies that may address hybrid and electric powered vehicles, multi-vehicle studies, and WUI fire hazard mitigation strategies.

CRediT authorship contribution statement

Giovanni Di Cristina: Writing – review & editing, Writing – original draft, Methodology, Investigation, Formal analysis, Data curation. **Aika Davis:** Writing – review & editing, Writing – original draft, Investigation, Formal analysis, Data curation. **Matthew Bundy:** Writing – review & editing, Supervision, Project administration, Methodology, Conceptualization. **Anthony Hamins:** Writing – review & editing, Supervision, Project administration, Methodology, Investigation, Conceptualization.

Declaration of competing interest

The authors declare that they have no known competing financial interests or personal relationships that could have appeared to influence the work reported in this paper.

Acknowledgments

The authors are grateful to Anthony Chakalis, Philip Deardorff, Marco Fernandez, and Justin Mills for their excellent technical assistance; Artur Chernovsky for preparing the versatile NFRL data acquisition system.

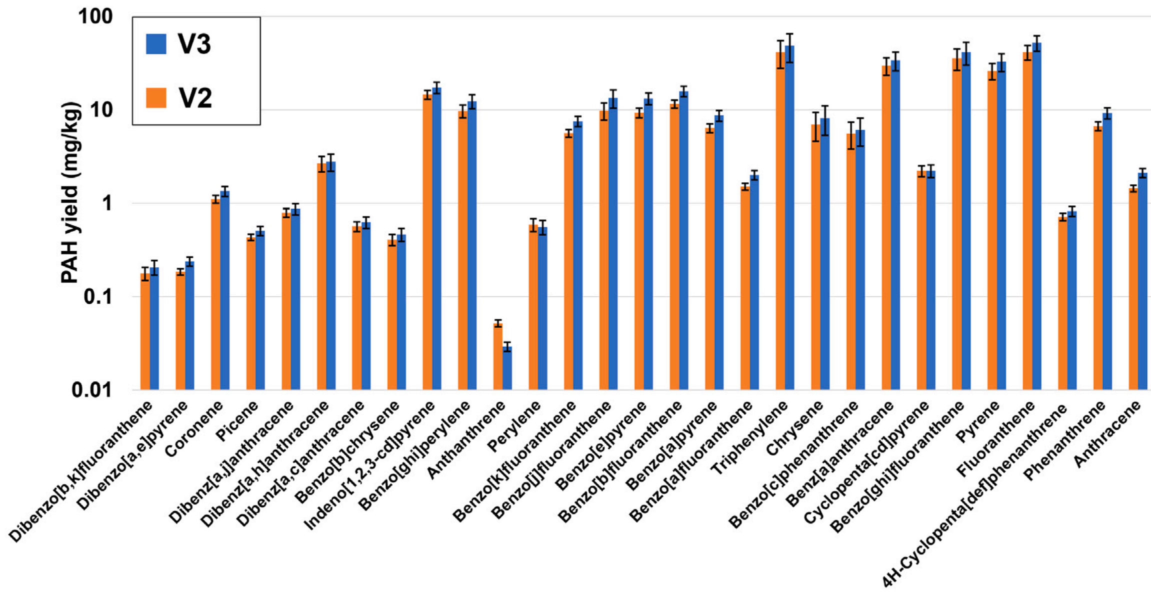

Fig. 13. Individual PAH yields per kg of mass loss for V2 and V3. The molecular weight of PAHs listed increase from right to left.

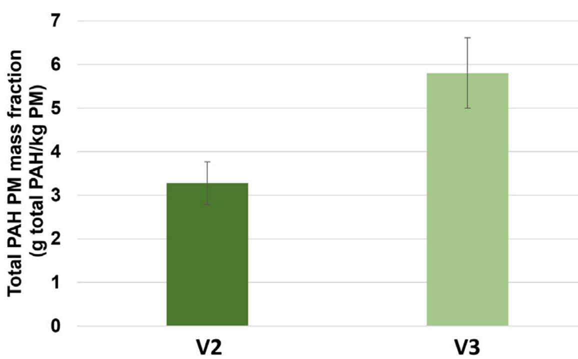

Fig. 14. Total PAH (anthracene equivalent) mass fraction per kg of PM for V2 and V3.

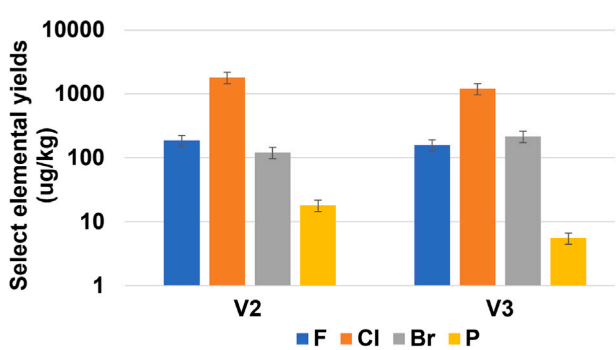

Fig. 15. Yields of F, Cl, Br, and P as PO4 in smoke from V2 and V3.

References

[1] Wenfu Tang, Cenlin He, Louisa Emmons, Junzhe Zhang, Global expansion of wildland-urban interface (WUI) and WUI fires: insights from a multiyear worldwide unified database (WUWUI), Environ. Res. Lett. 19 (4) (2024) 044028.

[2] National Interagency Coordination Center, National Interagency Coordination Center Wildland Fire Summary and Statistics Annual Report 2024, Technical Report 2024 Annual Report, NICC, Boise, Idaho, 2025.

[3] National Interagency Coordination Center, Federal firefighting suppression costs, 2025, https://www.nifc.gov/fire-information/statistics/suppression-costs.

[4] Alexander Maranghides, Eric Link, William "Ruddy" Mell, Steven Hawks, Mike Wilson, Will Brewer, Chris Brown, Bob Vihnaneck, William D. Walton, A Case Study of the Camp Fire – Fire Progression Timeline, Technical Report NIST TN 2135, National Institute of Standards and Technology, Gaithersburg, MD, 2021.

[5] Alexander Maranghides, Eric D Link, Steven Hawks, Jim McDougald, Stephen L Quarles, Daniel J Gorham, Shonali Nazare, WUI Structure/Parcel/Community Fire Hazard Mitigation Methodology, Technical Report NIST TN 2205, National Institute of Standards and Technology (U.S.), Gaithersburg, MD, 2022.

[6] Sara E. Caton, Raquel S.P. Hakes, Daniel J. Gorham, Aixi Zhou, Michael J. Gollner, Review of pathways for building fire spread in the wildland urban interface part I: Exposure conditions, Fire Technol. 53 (2) (2017) 429–473.

[7] Daryn Sagel, Kevin Speer, Scott Pokswinski, Bryan Quaife, Fine-scale fire spread in pine straw, Fire 4 (4) (2021) 69.

[8] Zakary Campbell-Lochrie, Carlos Walker-Ravena, Michael Gallagher, Nicholas Skowronski, Eric V. Mueller, Rory M. Hadden, Effects of fuel bed structure on heat transfer mechanisms within and above porous fuel beds in quiescent flame spread scenarios, Int. J. Wildland Fire (2023).

[9] Raquel S.P. Hakes, Sara E. Caton, Daniel J. Gorham, Michael J. Gollner, A review of pathways for building fire spread in the wildland urban interface part II: Response of components and systems and mitigation strategies in the united states, Fire Technol. 53 (2) (2017) 475–515.

[10] Xiao-hui Jiang, Guo-qing Zhu, Hui Zhu, Da-yan Li, Full-scale experimental study of fire spread behavior of cars, Procedia Eng. 211 (2018) 297–305.

[11] Jean-Baptiste Tramoni, Christophe Fraud, Mathieu Suzanne, Gildas Auguin, Christophe Thauvoye, Bin Zhao, Experimental investigation of the HRR of modern ICE vehicles, in: Proceedings from the Seventh International Conference on Fires in Vehicles, RISE Research Institutes of Sweden AB, Stavanger, Norway, 2023.

[12] Younggi Park, Jaiyoung Ryu, Hong Sun Ryou, Experimental study on the fire-spreading characteristics and heat release rates of burning vehicles using a large-scale calorimeter, Energies 12 (8) (2019) 1465.

[13] Dorota Brzezinska, Renata Ollesz, Paul Bryant, Design car fire size based on fire statistics and experimental data, Fire Mater. 44 (8) (2020) 1099–1107.

[14] Katsuhiro Okamoto, Norimichi Watanabe, Yasuaki Hagimoto, Tadaomi Chigira, Ryoji Masano, Hitoshi Miura, Satoshi Ochiai, Hideki Satoh, Yohsuke Tamura, Kimio Hayano, Yasumasa Maeda, Jinji Suzuki, Burning behavior of sedan passenger cars, Fire Saf. J. 44 (3) (2009) 301–310.

[15] Katsuhiro Okamoto, Takuma Otake, Hiroki Miyamoto, Masakatsu Honma, Norimichi Watanabe, Burning behavior of minivan passenger cars, Fire Saf. J. 62 (2013) 272–280.

[16] Mohd Mohd Tohir, Michael Spearpoint, Distribution analysis of the fire severity characteristics of single passenger road vehicles using heat release rate data, Fire Sci. Rev. 2 (1) (2013) 5.

[17] Bartosz Miechowka, Wojciech Wegrzynski, Systematic literature review on passenger car fire experiments for car park safety design, Fire Technol. 61 (4) (2025) 2651–2688.

[18] Rodney A. Bryant, Matthew F. Bundy, The NIST 20 MW Calorimetry Measurement System for Large-Fire Research, Technical Report NIST TN 2077, National Institute of Standards and Technology, Gaithersburg, MD, 2019.

[19] Haukur Ingason, Ulf Wickström, Measuring incident radiant heat flux using the plate thermometer, Fire Saf. J. 42 (2) (2007) 161–166.

[20] Ulf Wickström, Johan Anderson, Johan Sjöström, Measuring incident heat flux and adiabatic surface temperature with plate thermometers in ambient and high temperatures, Fire Mater. 43 (1) (2019) 51–56.
[21] George W. Mulholland, Erik L. Johnsson, Marco G. Fernandez, David A. Shear, Design and testing of a new smoke concentration meter, Fire Mater. 24 (5) (2000) 231–243.
[22] Giovanni Di Cristina, Ryan Falkenstein-Smith, Ickchan Kim, Savannah Wessies, Matthew Bundy, Mauro Zammarano, Towards fire safe and flame-retardant-free upholstered furniture, Proc. Combust. Inst. 40 (1–4) (2024) 105399.
[23] Aika Y. Davis, Thomas G. Cleary, Ryan L. Falkenstein-Smith, Rodney A. Bryant, Burning characteristics and smoke emission from mixed fuel cribs, ACS ES T Air 2 (4) (2025) 540–547.
[24] Aika Davis, Ryan Falkenstein-Smith, Thomas Cleary, Polycyclic Aromatic Hydrocarbons and Select Inorganics in Smoke from Various WUI Fire Fuels: Vehicles, Trees, and Construction Materials, Technical Report IN PRESS, National Institute of Standards and Technology (U.S.), Gaithersburg, MD, 2025.
[25] Aika Davis, Ryan Falkenstein-Smith, Thomas Cleary, Polycyclic Aromatic Hydrocarbon Analysis in Propene Smoke Using Thermal Desorption: Gas Chromatography - Mass Spectrometry, Technical Report NIST TN 2321, National Institute of Standards and Technology (U.S.), Gaithersburg, MD, 2024.
[26] Vytenis Babrauskas, W. Douglas Walton, A simplified characterization of upholstered furniture heat release rates, Fire Saf. J. 11 (3) (1986) 181–192.
[27] H. Ingason, Fire development in large tunnel fires, Fire Saf. Sci. 8 (2005) 1497–1508.
[28] Mohd Zahirasri Mohd Tohir, Michael Spearpoint, Charles Fleischmann, Probabilistic design fires for passenger vehicle scenarios, Fire Saf. J. 120 (2021) 103039.
[29] Jonathan L. Hodges, Urvin Salvi, Anil Kapahi, Design fire scenarios for hazard assessment of modern battery electric and internal combustion engine passenger vehicles, Fire Saf. J. 146 (2024) 104145.
[30] Ola Willstrand, Roeland Bisschop, Per Blomqvist, Alastair Temple, Johan Anderson, Toxic Gases from Fire in Electric Vehicles, Technical Report RISE Report 2020:90, RISE, 2020.
[31] Mohd Zahirasri Mohd Tohir, Michael Spearpoint, Charles Fleischmann, Prediction of time to ignition in multiple vehicle fire spread experiments, Fire Mater. 42 (1) (2018) 69–80.
[32] Yue Hu, Xiaodong Zhou, Junda Cao, Liang Zhang, Gang Wu, Lizhong Yang, Interpretation of fire safety distances of a minivan passenger car by burning behaviors analysis, Fire Technol. 56 (4) (2020) 1527–1553.
[33] H. Koseki, Large scale pool fires : Results of recent experiments, Fire Saf. Sci. 6 (2000) 115–132.
[34] Amara L Holder, Aranya Ahmed, Jeffrey M Vukovich, Venkatesh Rao, Hazardous air pollutant emissions estimates from wildfires in the wildland urban interface, in: Cristina H. Amon (Ed.), PNAS Nexus 2 (6) (2023) pgad186.
[35] Daniel A. Jaffe, Susan M. O'Neill, Narasimhan K. Larkin, Amara L. Holder, David L. Peterson, Jessica E. Halofsky, Ana G. Rappold, Wildfire and prescribed burning impacts on air quality in the United States, J. Air Waste Manage. Assoc. 70 (6) (2020) 583–615.
[36] C.N. Jen, L.E. Hatch, V. Selimovic, R.J. Yokelson, R. Weber, A.E. Fernandez, N.M. Kreisberg, K.C. Barsanti, A.H. Goldstein, Speciated and total emission factors of particulate organics from burning western US wildland fuels and their dependence on combustion efficiency, Atmos. Chem. Phys. 19 (2) (2019) 1013–1026.